H. J. Xu

Z. G. Qu[1]
e-mail: zgqu@mail.xjtu.edu.cn

MOE Key Laboratory of Thermo-Fluid
Science and Engineering,
Xi'an Jiaotong University,
710049, China

T. J. Lu
MOE Key Laboratory of Strength and Vibration,
Xi'an Jiaotong University,
710049, China

Y. L. He

W. Q. Tao

MOE Key Laboratory of Thermo-Fluid
Science and Engineering,
Xi'an Jiaotong University,
710049, China

Thermal Modeling of Forced Convection in a Parallel-Plate Channel Partially Filled With Metallic Foams

Fully developed forced convective heat transfer in a parallel-plate channel partially filled with highly porous, open-celled metallic foam is analytically investigated. The Navier–Stokes equation for the hollow region is connected with the Brinkman–Darcy equation in the foam region by the flow coupling conditions at the porous–fluid interface. The energy equation for the hollow region and the two energy equations of solid and fluid for the foam region are linked by the heat transfer coupling conditions. The normalized closed-form analytical solutions for velocity and temperature are also obtained to predict the flow and temperature fields. The explicit expression for Nusselt number is also obtained through integration. A parametric study is conducted to investigate the influence of different factors on the flow resistance and heat transfer performance. The analytical solution can provide useful information for related heat transfer enhancement with metallic foams and establish a benchmark for similar work. [DOI: 10.1115/1.4004209]

Keywords: metallic foams, heat transfer enhancement, porous-fluid interface, analytical solution

1 Introduction

There are many basic theories explaining heat transfer enhancement for internal flow, such as decreasing thickness of boundary layer, increasing velocity from laminar flow to turbulent flow, and increasing the extended surface area of the channel wall [1]. Among these, increasing the extended surface area of the channel wall is a commonly used method. Several ways of extending the surface have been put forward, such as finned [2], ribbed [3], slotted [4], chemically etched [5], porous-media adhered surfaces [6], etc.

As a special porous media, high porosity cellular metallic foam ($\varepsilon > 85\%$) has great potential in heat transfer enhancement. Its advantages are low density, high specific surface area, good flow-mixing ability, high thermal conductivity, and high strength. High porosity metallic foams, characterized by open cells as the extended surface to enhance heat transfer, can be applied in compact heat exchangers, heat sinks, catalyst supports, biomedical implants, and heat shield devices for space vehicles [7].

Forced convective heat transfer in ducts fully filled with metallic foams or other porous media has been extensively investigated. Lu et al. [7] have used the fin analogy method to estimate the forced convective heat transfer performance of metallic foam heat exchangers and heat sinks. According to their results, metallic foams have great potential in heat transfer enhancement. Calmidi and Mahajan [8] have conducted experimental and numerical studies on forced convection in a rectangular duct fully filled with metallic foams to analyze the effects of thermal dispersion and local nonthermal equilibrium with quantified thermal dispersion conductivity, k_d, and interstitial heat transfer coefficient, h_{sf}. Zhao et al. [9] have performed numerical and experimental investigation on forced convection in rectangular duct filled with metallic foams. The results of both studies mentioned above agree with each other very well. Lu and Zhao et al. [10,11] have analytically investigated flow and heat transfer in a single-pipe and in an annulus filled with metallic foams. They found that the foam morphology parameters (porosity and pore density) play important roles in heat transfer performance. Analytical studies with Darcy model were conducted by Mahjoob and Vafai [12] for the heat transfer in biological porous media and by Yang and Vafai [13] for a porous medium filled parallel-plate channel with heat generation.

Although metallic foams can substantially enhance heat transfer, they can also cause great pressure drop. To this end, configuration of ducts partially filled with metallic foams is proposed in this work. However, previous numerical and analytical works only focused on one-equation model with local thermal equilibrium (LTE) assumption for porous media partially filled channel. Numerical work using one-equation model was conducted by Chandesris [14] for the Poiseuille flow in a channel with a porous–fluid interface and by Vafai and Kim [15] for internal flow in a solar collector containing a porous–fluid interface. For analytical study, Vafai and Thiyagaraja [16] have obtained the approximate perturbation solutions of flow and heat transfer for the porous–fluid interface problem with one-equation model. Then, Poulikakos and Kazmierczak [17] and Chikh et al. [18] proposed analytical solution for forced convection in ducts partially filled with porous media and in a gap between two concentric cylinders with Brinkman–Darcy and one-equation models.

However, local thermal nonequilibrium (LTNE) is more accurate than LTE model, as indicated in Lee and Vafai [19], and two energy equations are required for present heat transfer process due to significant difference between thermal conductivities of solid and fluid. The two key challenges of analytical solutions are implementation of the two-equation model and coupling conditions at the porous–fluid interface. Based on this condition, variable number for temperature is extended to three including solid temperature, fluid temperatures in the foam region, and fluid temperature in the hollow region, respectively. The number of porous–fluid interface coupling conditions is also extended to three correspondingly. There are two main types of interface conditions for flow and heat transfer, namely, slip [14,15,20–22] and no-slip

[1]Corresponding author.

Contributed by the Heat Transfer Division of ASME for publication in the JOURNAL OF HEAT TRANSFER. Manuscript received October 7, 2010; final manuscript received May 8, 2011; published online July 27, 2011. Assoc. Editor: Sujoy Kumar Saha.

[16–18,20–23] conditions. Alazmi [20] reviewed different kinds of interfacial conditions related to velocity and temperature with the one-equation model. Even though there are only a few theoretical [24] or numerical [25,26] papers for heat transfer in a porous–fluid system with two-equation model, no analytical solution with two-equation model is available in open literature.

In this study, a mathematical model for fully developed forced convective heat transfer in a parallel-plate channel partially filled with metallic foams is established. By employing the Brinkman–Darcy and two-equation models, analytical investigation has been conducted with no-slip interface conditions. Transport behavior at the porous–fluid interface has been discussed, based on which, the Brinkman–Darcy and Navier–Stokes equations, as well as the two energy equations in foam region and the energy equation in hollow region, are linked together. Analytical solutions with explicit expressions for velocity, temperature profiles, and Nusselt number have been derived. A parametric study on effects of different parameters on flow and heat transfer has been conducted.

2 Mathematical Equations

2.1 Problem Description. Schematic diagram of the parallel-plate partially filled with metallic foams is shown in Fig. 1. Two isotropic and homogeneous metallic foam layers are symmetrically sintered on the upper and bottom plates subjected to uniform heat flux. Fluid is assumed to own constant thermal–physical properties. Thermal dispersion effect is neglected for metallic foams with high solid thermal conductivity according to Calmidi and Mahajan [8].

2.2 Simplified Equations. Given that flow and temperature fields of forced convection are fully developed, the following conditions hold

$$\frac{\partial}{\partial x}\left(\frac{T-T_w}{T_{f,b}-T_w}\right)=0 \tag{1}$$

$$\nu=0,\quad \frac{\partial u}{\partial x}=0,\quad \frac{\partial p}{\partial y}=0,\quad \frac{\partial p}{\partial x}=\text{const} \tag{2a}$$

$$\frac{dT_w}{dx}=\frac{dT_{f,b}}{dx}=\frac{\partial T_f}{\partial x}=\frac{\partial T_s}{\partial x}=\text{const} \tag{2b}$$

Axial heat conduction is accurately zero through deduction for fully developed forced convection. As the temperature field is fully developed, the local heat transfer coefficient h_x along the axial direction is unchanged. Thus, governing equations for the fluid and the foam regions are simplified as presented below.

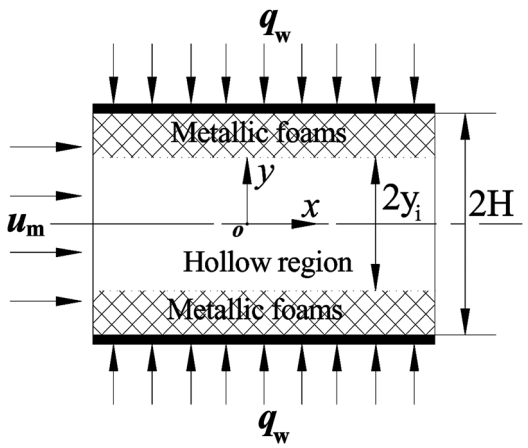

Fig. 1 Schematic diagram of a parallel-plate channel partially filled with metallic foam

Momentum and energy equations for the hollow region $(0 \le y \le y_i)$ are

$$\mu_f \frac{\partial^2 u}{\partial y^2}-\frac{dp}{dx}=0 \tag{3}$$

$$k_f \frac{\partial^2 T_f}{\partial y^2}=\rho_f c_f u \frac{\partial T_f}{\partial x} \tag{4}$$

Momentum and two energy equations for the foam region $(y_i \le y \le H)$ are

$$\frac{\mu_f}{\varepsilon}\frac{\partial^2 u_f}{\partial y^2}-\frac{\mu_f}{K}u_f-\frac{dp}{dx}=0 \tag{5}$$

$$k_{se}\frac{\partial^2 T_s}{\partial y^2}-h_{sf}a_{sf}(T_s-T_f)=0 \tag{6}$$

$$k_{fe}\frac{\partial^2 T_f}{\partial y^2}+h_{sf}a_{sf}(T_s-T_f)=\rho_f c_f u\frac{\partial T_f}{\partial x} \tag{7}$$

Using energy balance for the uniform heat flux condition, Eq. (8) holds

$$\rho_f u_m \cdot 2H \cdot c_f \cdot dT_{f,b}=2q_w \cdot dx \tag{8}$$

Combined with Eq. (8), Eqs. (4) and (7) are rewritten as Eqs. (9) and (10) for the convenience of normalization

$$k_f \frac{\partial^2 T_f}{\partial y^2}=\frac{q_w}{H}\frac{u}{u_m} \tag{9}$$

$$k_{fe}\frac{\partial^2 T_f}{\partial y^2}+h_{sf}a_{sf}(T_s-T_f)=\frac{q_w}{H}\frac{u}{u_m} \tag{10}$$

2.3 Closure Conditions. Closure conditions consist of boundary conditions and coupling conditions at the foam–fluid interface. Boundary conditions can be obtained as follows

$$y=0:\frac{du}{dy}=\frac{\partial T_f}{\partial y}=0 \tag{11}$$

$$y=H:u=0,T_s=T_f=T_w \tag{12}$$

Given that the two sets of governing equations are coupled at the porous–fluid interface, the interfacial coupling conditions need to be determined to close Eqs. (3)–(7). The continuities of velocity, shear stress, fluid temperature, and heat flux at the porous–fluid interface should be guaranteed for meaningful physics. The corresponding expressions are shown in Eqs. (13)–(16), respectively.

$$u|_{y_i^-}=u|_{y_i^+} \tag{13}$$

$$\mu_f \left.\frac{du}{dy}\right|_{y_i^-}=\left.\frac{\mu_f}{\varepsilon}\frac{du}{dy}\right|_{y_i^+} \tag{14}$$

$$T_f|_{y_i^-}=T_f|_{y_i^+} \tag{15}$$

$$k_f\left.\frac{\partial T_f}{\partial y}\right|_{y_i^-}=\left.\left(k_{fe}\frac{\partial T_f}{\partial y}+k_{se}\frac{\partial T_s}{\partial y}\right)\right|_{y_i^+} \tag{16}$$

There are three variables for two energy equations: the fluid and solid temperatures of the foam region and the temperature of the open region. Therefore, another coupling condition is needed for obtaining the temperature of solid and fluid in the foam region. Ochoa-Tapia and Whitaker [21] have put forward an interface condition for nonequilibrium heat transfer at the porous–fluid interface, as shown in

$$k_{se}\nabla T_s|_{y_i^+}=h_{sf}\left(T_s|_{y_i^+}-T_f|_{y_i^-}\right) \tag{17}$$

Table 1 Semi-empirical correlations of parameters for metallic foams

Parameter	Correlation	Reference
Pore diameter d_p	$d_p = 0.0254/\omega$	[29]
Fiber diameter d_f	$d_f = d_p \cdot 1.18\sqrt{(1-\varepsilon)/(3\pi)}[1-\exp((\varepsilon-1)/0.04)]^{-1}$	[29]
Specific surface area a_{sf}	$a_{sf} = \dfrac{3\pi d_f\left[1-e^{-((1-\varepsilon)/0.04)}\right]}{(0.59d_p)^2}$	[10]
Permeability K	$K = 0.00073(1-\varepsilon)^{-0.224}(d_f/d_p)^{-1.11}d_p^2$	[29]
Local heat transfer coefficient h_{sf}	$h_{sf} = \begin{cases} 0.76\mathrm{Re}_d^{0.4}\,\mathrm{Pr}^{0.37}\,k_f/d, & (1 \le \mathrm{Re}_d \le 40) \\ 0.52\mathrm{Re}_d^{0.5}\,\mathrm{Pr}^{0.37}\,k_f/d, & (40 \le \mathrm{Re}_d \le 10^3) \\ 0.26\mathrm{Re}_d^{0.6}\,\mathrm{Pr}^{0.37}\,k_f/d, & (10^3 \le \mathrm{Re}_d \le 2\times10^5) \end{cases}$ $\mathrm{Re}_d = \rho_f u d/\mu_f$	[10]
Effective thermal conductivity k_e	$R_A = \dfrac{4\lambda}{(2e^2+\pi\lambda(1-e))k_s + (4-2e^2-\pi\lambda(1-e))k_f}$	[30]
	$R_B = \dfrac{(e-2\lambda)^2}{(e-2\lambda)e^2k_s + (2e-4\lambda-(e-2\lambda)e^2)k_f}$	
	$R_C = \dfrac{(\sqrt{2}-2e)^2}{2\pi\lambda^2(1-2\sqrt{2}e)k_s + 2(\sqrt{2}-2e-\pi\lambda^2(1-2\sqrt{2}e))k_f}$	
	$R_D = \dfrac{2e}{e^2k_s + (4-e^2)k_f}$	
	$\lambda = \dfrac{\sqrt{\sqrt{2}(2-(5/8)e^3\sqrt{2}-2\varepsilon)}}{\pi(3-4\sqrt{2}e-e)}$, $e = 0.339$	
	$k_e = \dfrac{1}{\sqrt{2}(R_A+R_B+R_C+R_D)}$	
	$k_{se} = k_e\|_{k_f=0}$, $k_{fe} = k_e\|_{k_s=0}$	

For the reason that the axial heat conduction can be neglected for present study, Eq. (18) is simplified as

$$k_{se}\frac{\partial T_s}{\partial y}\bigg|_{y_i^+} = h_{sf}\left(T_s|_{y_i^+} - T_f|_{y_i^-}\right) \tag{18}$$

Due to the fact that the solid ligaments are discontinuous at the foam–fluid interface, heat conduction through the solid phase is totally transferred to the fluid in the manner of convective heat transfer across the foam–fluid interface. Thus, the physical meaning of Eq. (18) stands for the convective heat transfer at the foam–fluid interface from solid ligament to the fluid nearby. In the above, K, k_{se}, k_{fe}, a_{sf}, and h_{sf} are distinctive parameters for metallic foams and can be determined from Table 1.

3 Analytical Solution

3.1 Normalization. Dimensionless variables in governing equations and closure conditions are defined as follows

$$Y = \frac{y}{H}, Y_i = \frac{y_i}{H}, U = \frac{u}{u_m}, P = \frac{K}{\mu_f u_m}\frac{dp}{dx}, \theta_{f(s)} = \frac{T_{f(s)} - T_w}{q_w H/k_{se}} \tag{19a}$$

$$\mathrm{Da} = \frac{K}{H^2},\ A = \frac{h_{sf}H}{k_{se}},\ B = \frac{k_f}{k_{se}},\ C = \frac{k_{fe}}{k_{se}},\ D = \frac{h_{sf}a_{sf}H^2}{k_{se}}$$

$$s = \sqrt{\frac{\varepsilon}{\mathrm{Da}}},\ t = \sqrt{\frac{D(C+1)}{C}} \tag{19b}$$

The dimensionless governing equations for the hollow region ($0 \le Y \le Y_i$) are as follows

$$\frac{\partial^2 U}{\partial Y^2} - \frac{P}{\mathrm{Da}} = 0 \tag{20}$$

$$\frac{\partial^2 \theta_f}{\partial Y^2} = \frac{1}{B}U \tag{21}$$

The dimensionless governing equations for the foam region ($Y_i \le Y \le 1$) are as follows

$$\frac{\partial^2 U}{\partial Y^2} - s^2(U+P) = 0 \tag{22}$$

$$\frac{\partial^2 \theta_s}{\partial Y^2} - D(\theta_s - \theta_f) = 0 \tag{23}$$

$$C\frac{\partial^2 \theta_f}{\partial Y^2} + D(\theta_s - \theta_f) = U \tag{24}$$

Corresponding dimensionless closure conditions are as follows

$$Y = 0 : \frac{\partial U}{\partial Y} = \frac{\partial \theta_f}{\partial Y} = 0 \tag{25}$$

$$Y = 1 : U = 0, \theta_s = \theta_f = 0 \tag{26}$$

When $Y = Y_i$, the dimensionless coupling conditions are

$$U|_{Y_i^-} = U|_{Y_i^+} \tag{27a}$$

$$\frac{dU}{dY}\bigg|_{Y_i^-} = \frac{1}{\varepsilon}\frac{dU}{dY}\bigg|_{Y_i^+} \tag{27b}$$

$$\theta_f|_{Y_i^-} = \theta_f|_{Y_i^+} \tag{27c}$$

$$B\frac{\partial \theta_f}{\partial Y}\bigg|_{Y_i^-} = \left(C\frac{\partial \theta_f}{\partial Y} + \frac{\partial \theta_s}{\partial Y}\right)\bigg|_{Y_i^+} \tag{27d}$$

$$\frac{\partial \theta_s}{\partial Y}\bigg|_{Y_i^+} = A\left(\theta_s|_{Y_i^+} - \theta_f|_{Y_i^-}\right) \tag{27e}$$

3.2 Explicit Expressions

3.2.1 Velocity Distribution. The velocity field is typically obtained ahead of the temperature field for the uncoupled relationship between the momentum and energy equations. From Eqs. (20), (22), (25), (26), (27*a*), and (27*b*), velocity distribution in the hollow and foam regions are obtained. Velocity in the hollow region ($0 \le Y \le Y_i$) is expressed as

$$U = P\left(\frac{1}{2\mathrm{Da}}Y^2 + C_0\right) \tag{28}$$

Velocity in the foam region ($Y_i \le Y \le 1$) is expressed as

$$U = P\left(C_1 e^{sY} + C_2 e^{-sY} - 1\right) \tag{29}$$

With the closure conditions, the above constants C_0, C_1, and C_2 are determined as

$$C_0 = C_1 e^{sY_i} + C_2 e^{-sY_i} - Y_i^2/(2\mathrm{Da}) - 1 \tag{30a}$$

$$C_1 = \frac{e^{-sY_i} + sY_i e^{sY_i}}{e^{s(1-Y_i)} + e^{-s(1-Y_i)}} \tag{30b}$$

$$C_2 = \frac{e^{sY_i} - sY_i e^{s}}{e^{s(1-Y_i)} + e^{-s(1-Y_i)}} \tag{30c}$$

With continuity equation shown in Eq. (31*a*), the dimensionless pressure drop in the above solution is determined in Eq. (31*b*)

$$\frac{1}{A}\int_A UdA = 1. \tag{31a}$$

$$P = \frac{1}{\frac{1}{s}(C_1 e^{s} - C_2 e^{-s}) + \frac{Y_i^3}{6\mathrm{Da}} + C_0 Y_i - 1} \tag{31b}$$

Compared with the clear fluid region, the porous region with low permeability causes mass flow heterogeneity in the entire cross-section. The flow-characteristic difference between the two domains significantly influences the heat transfer performance. To reveal relationship between flow heterogeneity and heat transfer, a mass flow fraction in foam region, defined as ratio of mass flow rate in foam region to total mass flow rate, is shown as

$$\xi = \frac{q_{\mathrm{m,foam}}}{q_{\mathrm{m,total}}} = \frac{\int_{A_\mathrm{p}} UdA}{\int_A UdA} = \int_{Y_i}^{1} UdY = P\left(\frac{C_1 e^{s} - C_2 e^{-s}}{s} - 1\right) \tag{32}$$

3.2.2 Temperature Distribution. After combining the energy equations, Eqs. (21), (23), and (24), with the unique-solution conditions, Eqs. (25), (26), (27*c*), (27*d*), and (27*e*), dimensionless fluid temperature for the two regions and solid temperature for foam region can be interactively derived. In the hollow region ($0 \le Y \le Y_i$), dimensionless fluid temperature is

$$\theta_f = P \cdot \frac{1}{B}\left(\frac{1}{24\mathrm{Da}}Y^4 + \frac{C_0}{2}Y^2 + C_3\right) \tag{33}$$

In the foam region ($Y_i \le Y \le 1$), the dimensionless temperatures of fluid and solid are expressed as

$$\theta_s + C\theta_f = P\left[\frac{1}{s}\left(C_1 e^{sY} + C_2 e^{-sY}\right) - \frac{1}{2}Y^2 + C_4 Y + C_5\right] \tag{34}$$

$$\theta_f = P\left\{\begin{array}{l} C_6 e^{tY} + C_7 e^{-tY} + \frac{1-D/s^2}{C\cdot s^2 - D(C+1)}(C_1 e^{sY} + C_2 e^{-sY}) \\ -\frac{1}{2(C+1)}Y^2 + \frac{C_4}{C+1}Y + \frac{C_5}{C+1} + \frac{1}{D(C+1)^2} \end{array}\right\} \tag{35}$$

$$\theta_s = P\left\{\begin{array}{l} -\frac{1}{C}(C_6 e^{tY} + C_7 e^{-tY}) - \frac{D/s^2}{C\cdot s^2 - D(C+1)}(C_1 e^{sY} + C_2 e^{-sY}) \\ -\frac{1}{2(C+1)}Y^2 + \frac{C_4}{C+1}Y + \frac{C_5}{C+1} - \frac{C}{D(C+1)^2} \end{array}\right\} \tag{36}$$

The constants in the above equation are defined as

$$C_3 = B\left[\begin{array}{l} C_6 e^{tY_i} + C_7 e^{-tY_i} + \frac{1-D/s^2}{C\cdot s^2 - D(C+1)}(C_1 e^{sY_i} + C_2 e^{-sY_i}) \\ -\frac{1}{2(C+1)}Y_i^2 + \frac{C_4}{C+1}Y_i + \frac{C_5}{C+1} + \frac{1}{D(C+1)^2} \end{array}\right] - \frac{1}{24Da}Y_i^4 - \frac{C_0}{2}Y_i^2 \tag{37a}$$

$$C_4 = \frac{1}{6\mathrm{Da}}Y_i^3 + C_0 Y_i \tag{37b}$$

$$C_5 = \frac{1}{2} - \frac{1}{s^2} - C_4 \tag{37c}$$

$$C_6 = \frac{[A(C+1)+Ct]e^{-tY_i}C_8 - e^{-t}C_9}{[A(C+1)+Ct]e^{t(1-Y_i)} - [A(C+1)-Ct]e^{-t(1-Y_i)}} \tag{37d}$$

$$C_7 = \frac{e^{t}C_9 - [A(C+1)-Ct]e^{tY_i}C_8}{[A(C+1)+Ct]e^{t(1-Y_i)} - [A(C+1)-Ct]e^{-t(1-Y_i)}} \tag{37e}$$

$$C_8 = -\frac{C\cdot s^2}{D(C+1)^2[C\cdot s^2 - D(C+1)]} \tag{37f}$$

$$C_9 = A\left[-\frac{C_1 e^{sY_i} + C_2 e^{-sY_i}}{C\cdot s^2 - D(C+1)} - \frac{1}{D(C+1)}\right] - \frac{C\cdot s^2\cdot Y_i}{(C+1)[C\cdot s^2 - D(C+1)]} - \frac{C_4}{C+1} \tag{37g}$$

The bulk dimensionless temperature for fluid is constant and can be obtained through its definition

$$\begin{aligned}\theta_{f,b} =& \frac{\frac{1}{A}\int_A U\theta_f dA}{\frac{1}{A}\int_A UdA} = \int_0^{Y_i} U\theta_f dY + \int_{Y_i}^{1} U\theta_f dY \\ =& \frac{P^2}{B}\left[\frac{1}{336\mathrm{Da}^2}Y_i^7 + \frac{7C_0}{120\mathrm{Da}}Y_i^5 + \left(\frac{C_3}{\mathrm{Da}} + C_0^2\right)\frac{Y_i^2}{6} + C_0 C_3 Y_i\right] \\ &+ P^2\left\{\frac{C_1 C_6}{s+t}\left(e^{(s+t)} - e^{(s+t)Y_i}\right) + \frac{C_1 C_7}{s-t}\left(e^{(s-t)} - e^{(s-t)Y_i}\right)\right. \\ &- \frac{C_2 C_6}{(s-t)}\left(e^{-(s-t)} - e^{-(s-t)Y_i}\right) - \frac{C_2 C_7}{(s+t)}\left(e^{-(s+t)} - e^{-(s+t)Y_i}\right) \\ &+ \frac{N_1 C_1^2}{2s}\left(e^{2s} - e^{2sY_i}\right) - \frac{N_1 C_2^2}{2s}\left(e^{-2s} - e^{-2sY_i}\right) \\ &+ \frac{C_1}{s}\left[e^{s}\left(N_2 + N_3 - \frac{2N_2}{s} - N_1 + \frac{2N_2}{s^2} - \frac{N_3}{s} + N_4\right)\right. \\ &\left. - e^{sY_i}\left(N_2 Y_i^2 + \left(N_3 - \frac{2N_2}{s}\right)Y_i - N_1 + \frac{2N_2}{s^2} - \frac{N_3}{s} + N_4\right)\right] \\ &- \frac{C_2}{s}\left[e^{-s}\left(N_2 + N_3 + \frac{2N_2}{s} - N_1 + \frac{2N_2}{s^2} + \frac{N_3}{s} + N_4\right)\right. \\ &\left. - e^{-sY_i}\left(N_2 Y_i^2 + \left(N_3 + \frac{2N_2}{s}\right)Y_i - N_1 + \frac{2N_2}{s^2} + \frac{N_3}{s} + N_4\right)\right] \\ &- \frac{C_6}{t}\left(e^{t} - e^{tY_i}\right) + \frac{C_7}{t}\left(e^{-t} - e^{-tY_i}\right) - \frac{N_3}{3}\left(1 - Y_i^3\right) \\ &\left. - \frac{N_3}{2}\left(1 - Y_i^2\right) + (2N_1 C_1 C_2 - N_4)(1 - Y_i)\right\}\end{aligned} \tag{38}$$

In Eq. (38), the constants, N_1, N_2, N_3, and N_4 are expressed as

$$N_1 = \frac{1 - D/s^2}{C\cdot s^2 - D(C+1)}, \quad N_2 = -\frac{1}{2(C+1)},$$
$$N_3 = \frac{C_4}{C+1}, \quad N_4 = \frac{1}{D(C+1)^2} \tag{39}$$

3.2.3 Dimensionless Numbers. The friction factor number and Nusselt number for parallel-plate channel are defined as

$$f = \frac{dp/dx \cdot 4H}{\rho_f u_m^2/2} = \frac{32P}{\mathrm{Re}\cdot\mathrm{Da}} \tag{40}$$

$$\mathrm{Nu} = h\frac{4H}{k_f} = \frac{q_w}{T_w - T_{f,b}}\frac{4H}{k_f} = -\frac{4}{B\cdot\theta_{f,b}} \tag{41}$$

From the above solutions, the temperature profiles and the Nusselt number are influenced by P, s, t, C, D, and Y_i and eventually is the function of the thermal–physical properties of fluid and solid (k_f and k_s), foam morphology parameters (ε and ω), Reynolds number (Re), channel size (H), and hollow ratio (Y_i). To analyze

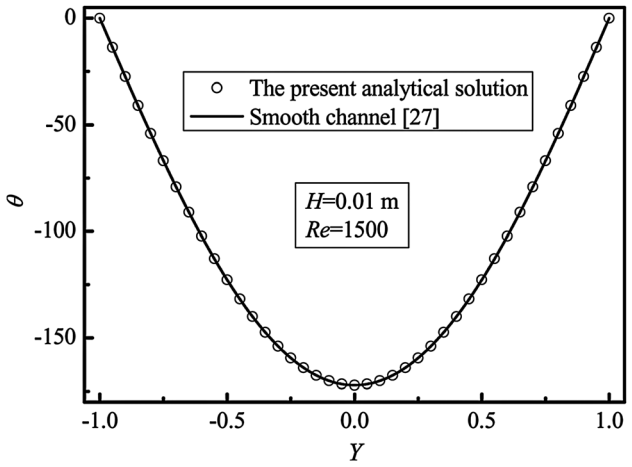

Fig. 2 Validation of the present analytical solution

integrated performance involving flow and heat transfer, the evaluation criteria is defined as

$$j/f^{1/3} = \frac{\mathrm{Nu}}{\mathrm{Re}(\mathrm{Pr}\cdot f)^{1/3}} \tag{42}$$

4 Parametric Study

4.1 Validation for Analytical Solution. The analytical solution can predict flow and heat transfer for various hollow ratios ranging from 0 to 1. The value $Y_i = 0$ corresponds to a channel fully filled with metallic foams and $Y_i = 1$ corresponds to an empty channel. By setting $Y_i \to 1$ (Fig. 2), temperature profile with present solution agrees well with similar smooth channel of previous work [27]. The good agreement shows the feasibility of the analytical solution.

4.2 Velocity Profile. The velocity profiles predicted by the analytical solutions shown in Eqs. (28), (29) at three combinations of porosity and pore density are presented in Fig. 3(*a*). It is found that the velocity in the hollow space is much higher than that in the foam region with obstructing foam ligaments. Increasing porosity or decreasing pore density can both increase velocity in foam region and decrease velocity in open region simultaneously since flow resistance in foam region can be reduced by increasing porosity and decreasing pore density of metallic foams.

Figure 3(*b*) illustrates the comparison of velocity profiles for four hollow ratios: 0 (foam fully filled channel); 0.2, 0.5, 0.8, and 1.0 (smooth channel). The velocity profile is parabolic distribution for the smooth channel and the profile for fully filled channel is similar except that the distribution is more uniform since no sudden change of permeability is in the cross-section. Comparatively for the foam partially filled channel, sudden change of permeability occurs at the porous–fluid interface, the average velocity in the central fluid region for foam partially filled channel ($Y_i = 0.2$, 0.5, 0.8) is higher than that of the foam fully filled channel and that of the empty channel and the maximum velocity in the central region decreases with increase of hollow ratio due to the big difference of permeability between porous and clear fluid regions. For comparison, velocity in the foam region of foam partially filled channel is much lower than that of foam fully filled channel and that of smooth channel.

4.3 Flow Heterogeneity. The existence of porous foam makes the permeability of the foam region much less than that of the open region, which implies that the velocity in the foam region is relative small even for a big frontal velocity. This fact just satisfies the present employment of Brinkman–Darcy model. The defined mass flow fraction in the foam region ξ is an important

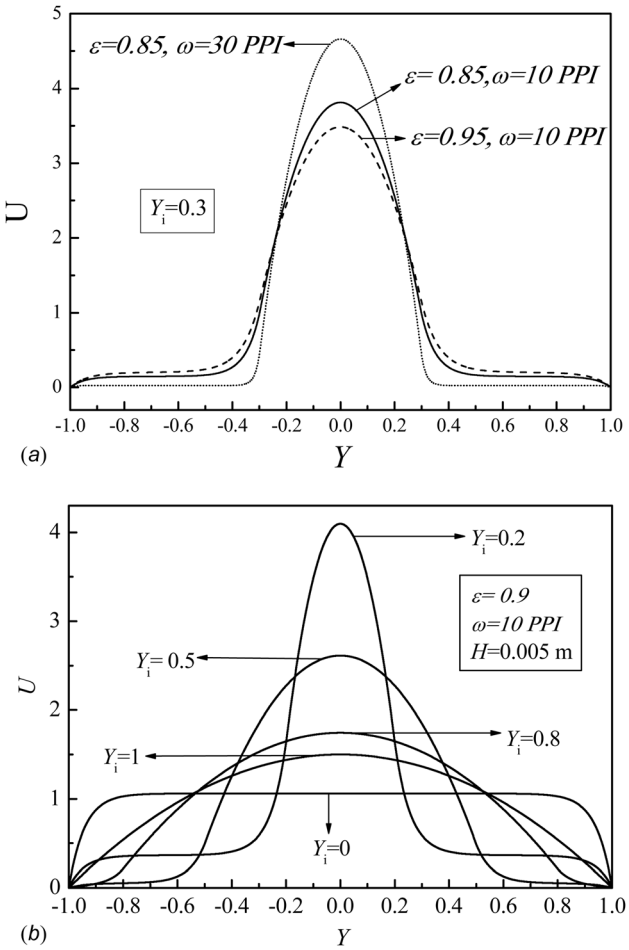

Fig. 3 Effect of key parameters on velocity profiles: (a) metal-foam morphology parameters and (b) hollow ratio

aspect to influence heat transfer. The effects of morphology and size parameters of metallic foams on ξ are examined and presented in this section.

With the Brinkman–Darcy model, mass flow fraction in the foam region is independent of the Reynolds number. Figure 4(*a*) presents the effect of hollow ratio on mass flow fraction in the foam region for different porosities with pore density 10 PPI. Initially, ξ sharply decreases from 1.0 to 0.1 when hollow ratio varies from 0 to about 0.2. Then, when Y_i changes from 0.2 to 1, ξ gradually approaches 0. This indicates that the turning point hollow ratio is about 0.2. When hollow ratio is greater than this value, the mass flow rate in the foam region is less than 10% of the total mass flow rate and the variation amplitude of ξ can be neglected. The increase in porosity leads to the thinner diameter of foam ligament at a fixed pore density, which will make the volume of obstructing solid $(1-\varepsilon)$ and flow resistance reduced. This can lead to that ξ slightly increases with an increase in porosity. Namely, mass flow fraction in the foam region is not sensitive to the porosity for the highly porous metallic foams.

Figure 4(*b*) presents the effect of pore density on mass flow fraction in the foam region for different hollow ratios with fixed porosity 0.95. Mass flow fraction in the foam region decreases as pore density increases because the flow resistance increases with an increase in pore density. Similarly, a turning point can be found on the $\xi - \omega$ curve. Beyond this point, the mass flow rate in the foam region can be almost neglected and that in the hollow region accounts for the majority of the total mass flow rate. With an increase in the hollow ratio, the pore density of the turning point decreases because flow resistance and flow area in foam region both decreased.

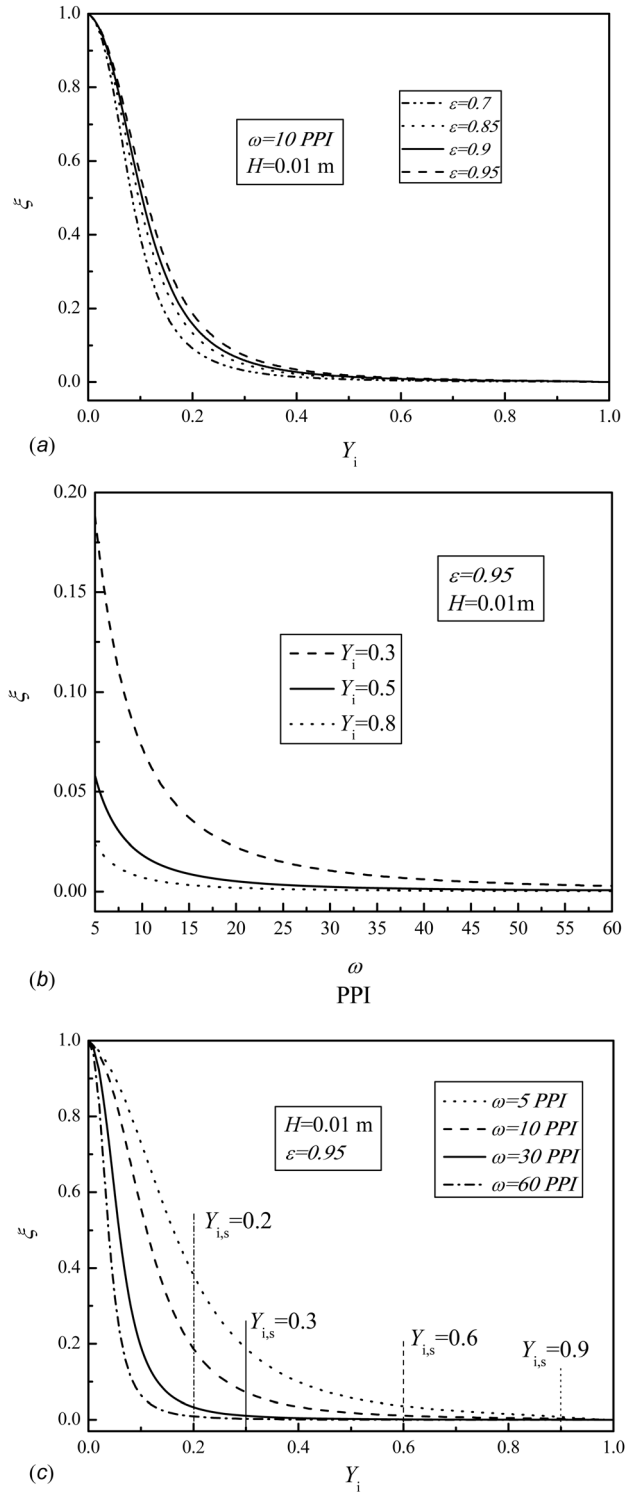

Fig. 4 Mass flow fraction in foam region: (a) as a function of hollow ratio for different porosities, (b) as a function of pore density for hollow ratios, and (c) as a function of hollow ratio for different pore densities

Figure 4(*c*) presents the effect of hollow ratio on ξ for different pore densities with fixed porosity 0.9. A saturation point $Y_{i,s}$ still exists and the saturation value decreases with an increase in pore density. It is noted that the pore density has more obvious effect on ξ compared with porosity, implying that the permeability of porous foam is very sensitive to the pore density rather than the porosity.

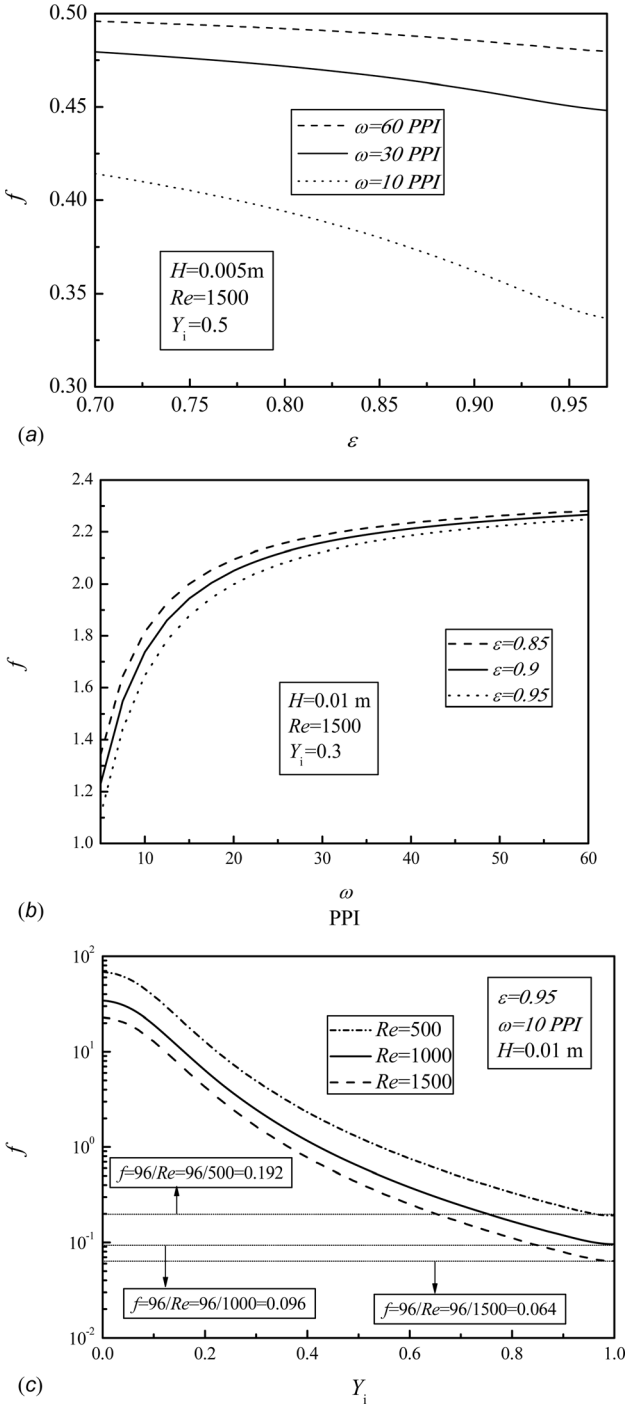

Fig. 5 Effect of key parameters on friction factor: (a) porosity, (b) pore density, and (c) hollow ratio

4.4 Friction Factor. As stated above, porosity, pore density, hollow ratio, and Reynolds number are all important factors influencing the flow characteristics. In this section, the effects of these parameters on friction factor are examined and presented in Fig. 5.

Figure 5(*a*) presents the effect of porosity on friction factor for different pore densities. As can be seen, the friction factor decreases with an increase in porosity. This is due to that an increase in porosity can result in the decreased solid volume fraction in the foam region and the relieved flow resistance. Figure 5(*b*) shows the effect of pore density on friction factor for different porosities. As pore density increases, the friction factor sharply increases for small pore density and then gradually

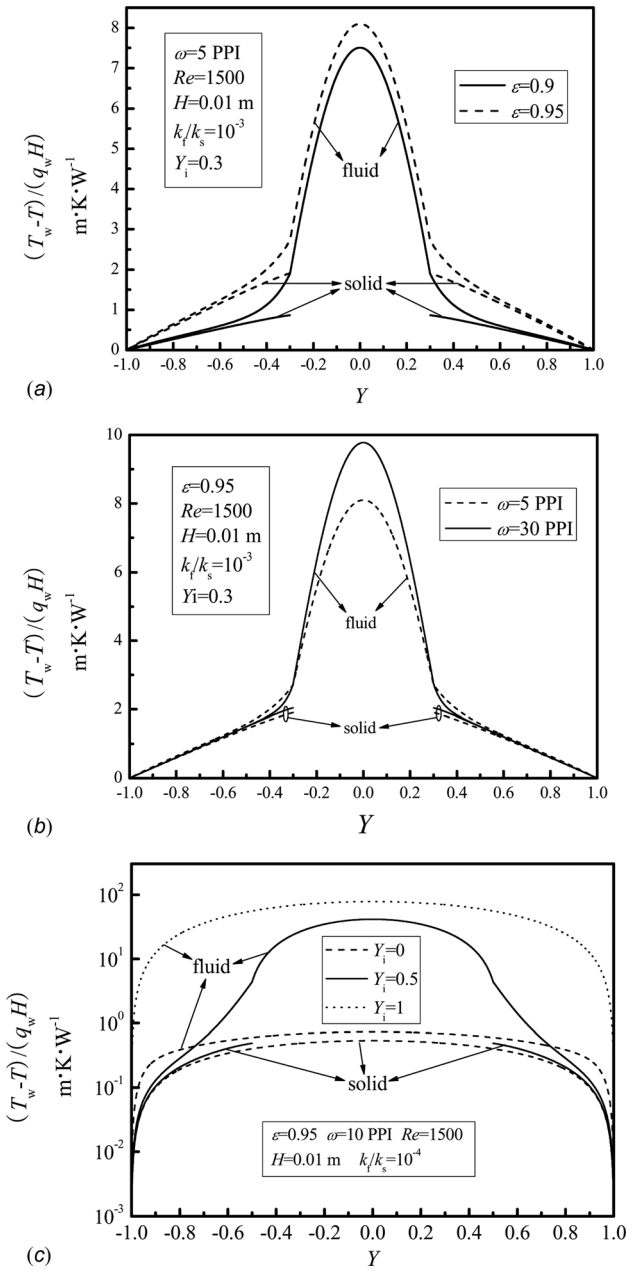

Fig. 6 Effect of key parameters on temperature profiles: (a) porosity, (b) pore density, and (c) hollow ratio

reaching a plateau when the pore density continues to increase. This could be attributed to the fact that mass flow fraction in the foam region becomes less than 2.5% when pore density is high enough (>20 PPI for $Y_i = 0.3$ from Fig. 4(*b*)), demonstrating the mild effect of the porous structure on flow resistance after the turning point of pore density. This phenomenon is quite different from that in the channel fully filled with metallic foams. Figure 5(*c*) presents the effect of hollow ratio on friction factor for different Reynolds number. It is found that the friction factor reduces with increase of Y_i. When Y_i approaches 1 as the smooth channel, all the friction factors for the different channel heights converged to the value for empty channel (96/Re) [27].

4.5 Temperature Profile. Based on the temperature distribution in Eqs. (33)–(36), the effects of porosity, pore density, and hollow ratio on temperature profiles are shown in Fig. 6. It should be noted that the effective thermal conductivity of solid k_{se} is used in the dimensionless temperature. However, k_{se} is influenced by foam morphology parameters from Table 1. To diminish effect of k_{se} on temperature for different foam morphologies, a nominal excess temperature θ/k_{se} $((T_w - T)/(q_w H))$ was used to represent the temperature instead of θ as indicated in Ref. [10].

Figure 6(*a*) presents the influence of porosity on temperature profile. As can be seen, the nominal excess temperature of fluid in the hollow region decreases in the y direction and the decreasing trend becomes less obvious in the foam region. This is due to that the total thermal resistance in the foam region is lower than that in the hollow region for the significant heat transfer surface extension. The nominal excess temperatures of fluid and solid in the foam region for $\varepsilon = 0.9$ were lower than that for $\varepsilon = 0.95$ because the decreased porosity leads to the increase in both the effective thermal conductivity and the foam surface area to improve the corresponding heat transfer with the same heat flux.

The effect of pore density on temperature profile is shown in Fig. 6(*b*). The solid excess temperature is almost the same in the foam region for different pore densities. This is attributed to that the heat conduction thermal resistance of the foam is mainly affected by porosity from Table 1. On the other hand, the nominal excess fluid temperature for 5 PPI is significantly smaller than that for 30 PPI. The trend inconsistency of the fluid and solid temperatures in the two regions for the two pore densities is caused by mass flow fraction in the foam region. The local convective heat transfer coefficient for 5 PPI was higher than 30 PPI due to the relative higher mass flow fraction in the foam region as indicated in Fig. 4(*b*). However, the heat transfer surface area inside the foam for 5 PPI is lower than that for 30 PPI. The two opposite effects competed with each other, resulting in the identical temperature difference between wall and fluid in the foam region. However, in the hollow region, the porous–fluid interface area becomes the only surface area, which is the same for the two pore densities under the same porosity. Hence, the temperature difference between wall and fluid for 5 PPI is reduced and obviously lower than that for 30 PPI.

Figure 6(*c*) presents the comparison of fluid and solid temperature distribution for different channels, including empty channel ($Y_i = 1$), foam partially filled channel ($Y_i = 0.5$), and foam fully filled channel ($Y_i = 0$). The nominal excess temperature becomes dependent on the heat transfer area and local heat transfer coefficient. In the hollow region, the heat transfer surface area is reduced to the interface area for foam partially filled channel ($Y_i = 0.5$), which was much smaller than the volume surface area of the fully filled channel ($Y_i = 0$). The nominal fluid excess temperature increases in the order of $Y_i = 1.0$, $Y_i = 0.5$, and $Y_i = 0$ since the total convective thermal resistance $1/(ha_{sf})$ decreases in the order $Y_i = 0$, $Y_i = 0.5$, nd $Y_i = 1.0$ in the clear fluid region. In the near-wall foam region, the mass flow rate accounts for about 2.5% of the total mass flow rate (Fig. 4(*b*)) and the local heat transfer coefficient for $Y_i = 0.5$ is reduced compared with that for $Y_i = 0$. However, the effect of fluid heat conduction dominates in the near-wall area, resulting in that the nominal fluid excess temperature for $Y_i = 0.5$ is lower than that for foam fully filled channel ($Y_i = 0$). Thus, an intersection point occurs in the curve of the fluid excess temperature distribution.

4.6 Heat Transfer Performance. Figure 7(*a*) presents the effect of porosity on Nu for four different metal materials: steel, nickel, aluminum, and copper with air as working fluid. The Nusselt number does not monotonically increase with porosity increase and a maximum value of Nu exists at a critical porosity. This can be attributed to the fact that increasing porosity will lead to a decrease in effective thermal conductivity and an increase in mass flow rate in the foam region. Below the critical porosity, the increase of the mass flow region prevails and Nu increases to the maximum value. When the porosity is higher than the critical value, which approaches 1, the decrease of thermal conductivity prevails. The Nusselt number sharply reduces and approaches the

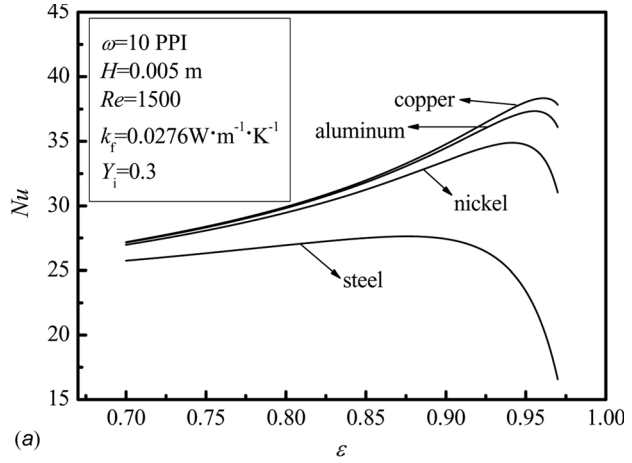

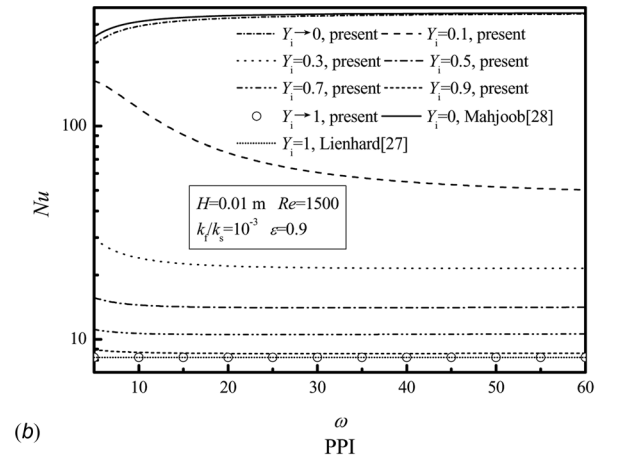

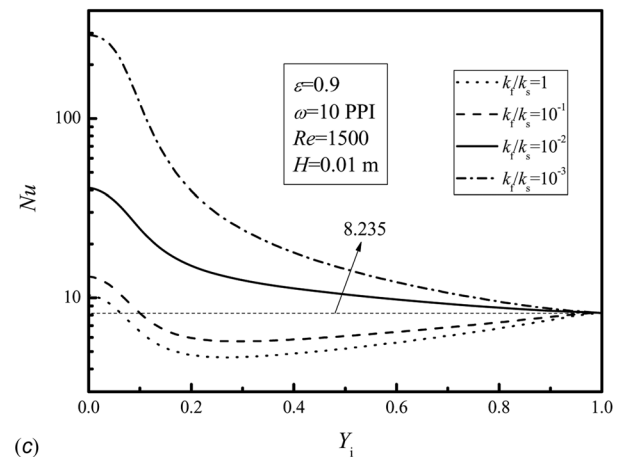

Fig. 7 Effect of key parameters on the Nusselt number: (a) porosity, (b) pore density, and (c) hollow ratio

value of the smooth channel. It is observed that the increase in the solid thermal conductivity can result in an increase in Nu. The critical porosity also increases with the solid thermal conductivity. It is implied that porosity should be kept at an optimal value in the design of related heat transfer devices in order to maximize the heat transfer coefficient.

Figure 7(*b*) shows the effect of pore density on Nu for different hollow ratios in which the two limiting cases for $Y_i = 1$ of Lienhard et al. [27] and $Y_i = 0$ of Mahjoob and Vafai [28] are compared as references. As Y_i approaches 1, the predicted Nu of the present analytical solution, with a value of 8.235, coincides accurately with that of the smooth channel of Lienhard et al. [27]. As

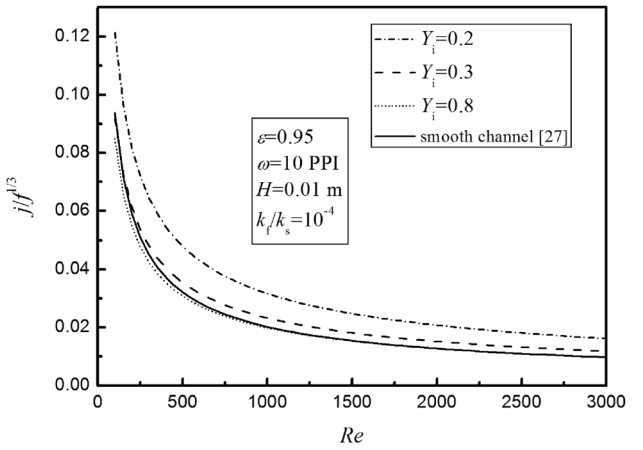

Fig. 8 Effect of Reynolds number on comprehensive performance for different hollow ratios

Y_i approaches 0, the difference between present analytical result and Mahjoob and Vafai [28] is very mild since the effect of viscous force of impermeable wall is considered in the present work and not considered in Ref. [28] with Darcy model. This provides another evidence for the feasibility of the present analytical solution. It is also found that the Nusselt number gradually decreases to a constant value as pore density increases. Increasing pore density can improve the heat transfer surface area but can lead to drastic deduction of mass flow rate in the foam region since ξ decreases to less than 2% in the foam region when the pore density is higher than 30 PPI as seen in Fig. 4(*b*). Hence, small pore density is recommended to maintain heat transfer performance and to reduce pressure drop for thermal design of related applications.

The effect of hollow ratio on Nu under various k_f/k_s is shown in Fig. 7(*c*). At high k_f/k_s ($1, 10^{-1}$), a minimized Nu exists as Y_i varies from 0 to 1, which is in accordance with the thermal equilibrium result of Poulikakos and Kazmierczak [17]. However, Nu monotonically decreases as Y_i varies from 0 to 1 for low k_f/k_s, as is the case for metallic foams with high solid thermal conductivities. This is attributed to that both the mass flow rate and foam surface area in the foam region reduce as Y_i increases. As Y_i approaches 1, Nusselt number gradually converge to the value 8.235, which is the exact value of forced convective heat transfer in smooth channel ($Y_i = 1$).

To investigate the comprehensive performance of foam partially filled channel considering both heat transfer enhancement and pressure drop penalty. Figure 8 presents the effect of Reynolds number on the comprehensive performance for different hollow ratios with $j/f^{1/3}$ as the evaluation criteria. It is found that $j/f^{1/3}$ for $Y_i < 0.3$ is higher than that for empty tube in present Reynolds number range. Thus, the hollow fraction less than 0.3, which own comprehensive heat transfer performance, can be recommended for practical application.

5 Conclusions

By adopting closure conditions for flow and heat transfer at foam–fluid interface, the Brinkman–Darcy and Navier–Stokes equations, as well as the two energy equations for the foam region and the energy equation for the clear fluid region, have been linked together. Analytical solutions for velocity and temperature are proposed. Explicit expressions for friction factor and Nusselt number are derived. To reveal cross-sectional flow heterogeneity of foam partially filled channel, mass flow fraction in foam region is proposed, which is significantly affected by the hollow ratio. There exists a saturation hollow ratio after which ξ decreases to a level less than 10%. Moreover, ξ is more sensitive to the pore density than porosity. Flow resistance can be reduced by increasing

porosity, reducing pore density, and decreasing hollow ratio. Friction factor grows to a plateau when pore density becomes higher than a certain value. An optimal porosity exists, at which maximum heat transfer performance is obtained as porosity increases. However, heat transfer is deteriorated by increasing pored density, implying that small pore density should be recommended. Taking heat transfer enhancement and pressure penalty into account, the hollow fraction range $Y_i < 0.3$ offers superior comprehensive performance with higher $j/f^{1/3}$ compared with empty channel.

Acknowledgment

This work is supported by National Key Projects of Fundamental R/D of China (973 Project: Grant No. 2011CB610306) and National Natural Science Foundation of China (Grant No. 50806057).

Nomenclature

a_{sf} = specific surface area, m^{-1}
c_f = specific heat capacity of fluid, $\mathrm{J \cdot kg^{-1} \cdot K^{-1}}$
Da = Darcy number
f = friction factor
h = heat transfer coefficient, $\mathrm{W \cdot m^{-2} \cdot K^{-1}}$
h_{sf} = local heat transfer coefficient at solid-fluid contacting surface, $\mathrm{W \cdot m^{-2} \cdot K^{-1}}$
H = one half of the channel height, m
j = j factor
k = thermal conductivity, $\mathrm{W \cdot m^{-1} \cdot K^{-1}}$
K = permeability, $\mathrm{m^2}$
Nu = Nusselt number, $\mathrm{Nu} = h \cdot 4H/k_\mathrm{f}$
p = pressure, $\mathrm{N \cdot m^{-2}}$
P = dimensionless pressure drop
Pr = Prandtl number
q_m = mass flow, $\mathrm{kg \cdot s^{-1}}$
q_w = heat flux, $\mathrm{W \cdot m^{-2}}$
Re = Reynolds number, $\mathrm{Re} = \rho_\mathrm{f} u_\mathrm{m} 4H/\mu_\mathrm{f}$
T = temperature, K
u, v = x, y velocity components, $\mathrm{m \cdot s^{-1}}$
u_m = mean velocity, $\mathrm{m \cdot s^{-1}}$
U = dimensionless u velocity
x, y = Cartesian coordinates, m
y_i = interface location in y direction, m
Y = dimensionless y coordinate
Y_i = dimensionless interface location, i.e., the hollow ratio

Greek Symbols

ε = porosity
ξ = mass flow fraction in the foam region
ω = pore density, PPI
μ = dynamic viscosity, $\mathrm{kg \cdot m^{-1} \cdot s^{-1}}$
θ = dimensionless temperature
ρ = density, $\mathrm{kg \cdot m^{-3}}$

Subscripts

b = bulk
e = effective
f = fluid
i = interface
s = solid/saturation

References

[1] Webb, R. L., and Kim, N. H., 1994, *Principles of Enhanced Heat Transfer*, 2nd ed., Wiley, New York.
[2] Wang, Q. W., Lin, M., and Zeng, M., 2009, "Effect of Lateral Fin Profiles on Turbulent Flow and Heat Transfer Performance of Internally Finned Tubes," Appl. Therm. Eng., **29**(14–15), pp. 3006–3013.
[3] Almeida, J. A., and Mendes, P. R., 1992, "Local and Average Transport Coefficients for the Turbulent Flow in Internally Ribbed Tubes," Exp. Therm. Fluid Sci., **5**(4), pp. 513–523.
[4] Evtushenko, I. A., Hua, T. Q., Kirillov, I. R., Reed, C. B., and Sidorenkov, S. S., 1995, "The Effect of a Magnetic Field on Heat Transfer in a Slotted Channel," Fusion Eng. Des., **27**(1), pp. 587–592.
[5] Wei, J. J., Gu, L. J., and Honda, H., 2005, "Experimental Study of Boiling Phenomena and Heat Transfer Performances of FC-72 Over Micro-Pin-Finned Silicon Chips," Heat Mass Transfer., **41**(8), pp. 744–755.
[6] Nield, D. A., and Bejan, A., 1992, *Convection in Porous Media*, 2nd ed., Springer, New York.
[7] Lu, T. J., Stone, H. A., and Ashby, M. F., 1998, "Heat Transfer in Open-Cell Metal Foams," Acta Mater., **46**(10), pp. 3619–3635.
[8] Calmidi, V. V., and Mahajan, R. L., 2000, "Forced Convection in High Porosity Metal Foams," ASME J. Heat Transfer, **122**(3), pp. 557–565.
[9] Zhao, C. Y., Kim, T., Lu, T. J., and Hodson, H. P., 2004, "Thermal Transport in High Porosity Cellular Metal Foams," AIAA J. Thermophys. Heat Transfer, **18**(3), pp. 309–317.
[10] Lu, W., Zhao, C. Y., and Tassou, S. A., 2006, "Thermal Analysis on Metal-Foam Filled Heat Exchangers. Part I: Metal-Foam Filled Pipes," Int. J. Heat Mass Transfer, **49**(15–16), pp. 2751–2761.
[11] Zhao, C. Y., Lu, W., and Tassou, S. A., 2006, "Thermal Analysis on Metal-Foam Filled Heat Exchangers. Part II: Tube Heat Exchangers," Int. J. Heat Mass Transfer, **49**(15–16), pp. 2762–2770.
[12] Mahjoob, S., and Vafai, K., 2010, "Analysis of Bioheat Transport Through a Dual Layer Biological Media," ASME J. Heat Transfer, **132**(3), 031101.
[13] Yang, K., and Vafai, K., 2010, "Analysis of Temperature Gradient Bifurcation in Porous Media—An Exact Solution," Int. J. Heat Mass Transfer, **53**(19–20), pp. 4316–4325.
[14] Chandesris, M., and Jamet, D., 2006, "Boundary Conditions at a Planar Fluid–Porous Interface for a Poiseuille Flow," Int. J. Heat Mass Transfer, **49**(13–14), pp. 2137–2150.
[15] Vafai, K., and Kim, S. J., 1990, "Analysis of Surface Enhancement by a Porous Substrate," ASME J. Heat Transfer, **112**(3), pp. 700–706.
[16] Vafai, K., and Thiyagaraja, R., 1987, "Analysis of Flow and Heat Transfer at the Interface Region of a Porous Medium," Int. J. Heat Mass Transfer, **30**(7), pp. 1391–1405.
[17] Poulikakos, D., and Kazmierczak, M., 1987, "Forced Convection in Duct Partially Filled With a Porous Material," ASME J. Heat Transfer, **109**(3), pp. 653–662.
[18] Chikh, S., Boumedien, A., Bouhadef, K., and Lauriat, G., 1995, "Analytical Solution of Non-Darcian Forced Convection in an Annular Duct Partially Filled With a Porous Medium," Int. J. Heat Mass Transfer, **38**(9), pp. 1543–1551.
[19] Lee, D. Y., and Vafai, K., 1999, "Analytical Characterization and Conceptual Assessment of Solid and Fluid Temperature Differentials in Porous Media," Int. J. Heat Mass Transfer, **42**(21), pp. 423–435.
[20] Alazmi, B., and Vafai, K., 2001, "Analysis of Fluid Flow and Heat Transfer Interfacial Conditions Between a Porous Medium and a Fluid Layer," Int. J. Heat Mass Transfer, **44**(9), pp. 1735–1749.
[21] Ochoa-Tapia, J. A., and Whitaker, S., 1995, "Momentum Transfer at the Boundary Between a Porous Medium and a Homogeneous Fluid—I: Theoretical Development," Int. J. Heat Mass Transfer, **38**(14), pp. 2635–2646.
[22] Ochoa-Tapia, J. A., and Whitaker, S., 1995, "Momentum Transfer at the Boundary Between a Porous Medium and a Homogeneous Fluid—II: Comparison With Experiment," Int. J. Heat Mass Transfer, **38**(14), pp. 2647–2655.
[23] Vafai, K., and Kim, S. J., 1995, "On the Limitations of the Brinkman-Forchheimer-Extended Equation," Int. J. Heat and Fluid Flow, **16**(1), pp. 11–15.
[24] Ochoa-Tapia, J. A., and Whitaker, S., 1997, "Heat Transfer at the Boundary Between a Porous Medium and a Homogeneous Fluid," Int. J. Heat Mass Transfer, **40**(11), pp. 2691–2707.
[25] Phanikumar, M. S., and Mahajan, R. L., 2002, "Non-Darcy Natural Convection in High Porosity Metal Foams," Int. J. Heat Mass Transfer, **45**(18), pp. 3781–3793.
[26] Yang, J., Zeng, M., Wang, Q. W., and Nakayama A., 2010, "Forced Convection Heat Transfer Enhancement by Porous Pin Fins in Rectangular Channels," ASME J. Heat Transfer, **132**(5), pp. 05172.1–05172.8.
[27] Lienhard, J. H. IV, and Lienhard J. H. V, 2006, *A Heat Transfer Textbook*, 3rd ed., Phlogiston Press, Cambridge.
[28] Mahjoob, S., and Vafai, K., 2009, "Analytical Characterization of Heat Transport Through Biological Media Incorporating Hyperthermia Treatment," Int. J. Heat Mass Transfer, **52**(5–6), pp. 1608–1618.
[29] Calmidi, V. V., 1998, *Transport Phenomena in High Porosity Fibrous Metal Foams*, Ph.D. thesis, University of Colorado.
[30] Boomsma, K., and Poulikakos, D., 2001, "On the Effective Thermal Conductivity of a Three-Dimensionally Structured Fluid-Saturated Metal Foam," Int. J. Heat Mass Transfer, **44**(4), pp. 827–836.